Volt/Var Optimization with Minimum Equipment Operation under High PV Penetration

Ibrahim Alsaleh
Electrical Engineering Department
University of South Florida,
Tampa, FL 33620, USA
Email: ialsaleh@mail.usf.edu

Lingling Fan
Electrical Engineering Department
University of South Florida,
Tampa, FL 33620, USA
Email: linglingfan@usf.edu

Hossein Ghassempour Aghamolki
Eaton Corporate Research & Technology
Eden Prairie, MN 55344
Email: hossein1@mail.usf.edu

***Abstract*—High penetration of photo-voltaic panels (PVs) in the distribution networks causes volatile net load profiles. In turn, voltage control devices (switched capacitors, on-load tap changers (OLTCs) and voltage regulators) work more frequently to keep voltage on distribution feeders within limits. This paper employs the most recently developed mixed-integer programming (MIP) modeling methods to model discrete control devices including OLTCs and switching capacitors for volt/var optimization to explicitly count mechanical switching actions. Further, coordination capability is explored to demonstrate that the use of PV VARs can effectively reduce operations of OLTCs and switched capacitors while obtaining a satisfactory voltage profile. Case studies are performed on the IEEE 33-node distribution feeder with 125% PV penetration.**

I. Introduction

Distributed generators (DGs) based on renewable energy have been increasingly integrated into the distribution networks. The excessive and intermittent nature of their power production adversely impacts the operation of the electrical system, causing large and sudden fluctuations of voltages. This problem is traditionally dealt with by employing switchable voltage regulation equipment comprising on-load tap changers (OLTCs), voltage regulators (VRs) and switched capacitor banks (SCBs) for voltage support and reactive power compensation. Although they are designed for a large number of annual operations, the repetitive switching to cope with the sharp voltage sags and swells will increase maintenance costs and expedite the wear and tear of these devices [1], [2].

The volt/var optimization (VVO) with traditional equipment sets the optimal tap position and/or capacitive reactive power to keep voltage levels within the $\pm 5\%$ limits specified by ANSI C84.1. Recently, standards such as IEEE 1547 allowed DG inverters to function with off-unity power factor, and thus participate in voltage regulation through reactive power generation/absorption. Smart technologies with two-way communication channels such as Advanced Metering Infrastructure (AMI) are deployed for capturing the distribution dynamic changes and enabling the operator at the Distribution Management System (DMS) to perform VVO and send control commands in a centralized manner [3].

The optimization problem is routinely solved by minimizing the real power losses. However, this increases the voltage level to the upper bound, unless being coordinated with other objectives such as Conservation of Voltage Reduction (CVR) [4], or minimization of voltage deviations from the nominal value [5].

Various methods have been developed on how off-unity inverters should support the voltage [6]. One method is to scale the reactive power supply/absorption linearly with respect to deviations of the local voltage [7], [8]. Another method is to set a strictly-fixed power factor on the inverter, where a fixed percentage of reactive power can be supplied/absorbed. Fig. 1 shows the operating points of the inverter adopted in this paper, which is an oversized inverter (110% of PV's rating $|S|_{\max}$) with a variable leading/lagging power factor. The reactive power, generated or absorbed during peak, is 46% of $|S|_{\max}$.

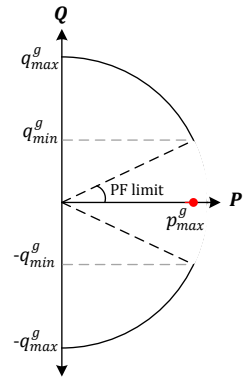

Fig. 1: Operating points of an oversized PV inverter.

This paper investigates the OLTC and SCB operations during high penetration of PV. A centralized VVO is formulated to switch conventional devices in order to prevent severe voltage fluctuations. Some voltage-dependent loads are configured, whose voltages should be kept at the lower-half as per CVR practices. For this, an additional objective is considered to further minimize the corresponding voltage. This would prompt the OLTC, SCBs and inverters to combat the variable penetration by changing tap positions and generating/absorbing VARs to satisfy the objective. However, poor coordination among the various devices results in increased operations of the OLTC and CBs.

Our contribution is a multi-period and multi-objective VVO that improves the voltage profile with a coordinated operation of conventional devices and PV VARs. Two notable techniques are adopted in our modeling: the SOCP relaxation technique for the branch flow model (BFM) which solves the problem to a global optimum [9], and the mixed-integer programming (MIP) technique to mimic the exact switching behavior of an OLTC and SCBs in response to voltage deviations from

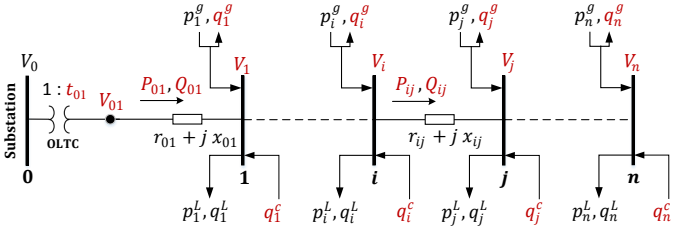

Fig. 2: A one-line diagram of a balanced radial distribution feeder and system variables.

desired.

The rest of the paper is organized as follows. Section II formulates the VVO problem. The equality and inequality constraints related to the BFM and system models as well as the objective function are presented successively. Section III conducts case studies to demonstrate the operation of OLTC and CB with and without the coordination. Section IV concludes the paper.

II. Centralized VVO Formulation

The nonlinear branch flow model describing the balanced power flow in a radial network was first proposed in [10], and was later convexified in [9]. Only recently has the MIP-based OLTC model been embedded in the convex relaxation of the branch flow model [11]–[13].

Fig. 2 shows a radial distribution feeder represented by the graph $\mathcal{G}(\mathcal{N}, \mathcal{E})$, where $\mathcal{N}$ and $\mathcal{E}$ correspond to the sets of nodes and branches; respectively. A fictitious node is assumed at the transformer primary to describe the power flow into the branch (i, j), and set relations among variables.

A. Constraints

1) BFM: Equations in (1) are expressed for (i, j)

$$P_{ij} = \sum_{k:(j,k)\in\mathcal{E}} P_{jk} + r_{ij}\ell_{ij} + p_j^L - p_j^g \tag{1a}$$

$$Q_{ij} = \sum_{k:(j,k)\in\mathcal{E}} Q_{jk} + x_{ij}\ell_{ij} + q_j^L - q_j^g - q_j^c \tag{1b}$$

$$v_j = v_i - 2(r_{ij}P_{ij} + x_{ij}Q_{ij}) + (r_{ij}^2 + x_{ij}^2)\ell_{ij} \tag{1c}$$

$$\ell_{ij} = (P_{ij}^2 + Q_{ij}^2)/v_{it} \tag{1d}$$

where P_{ij}, Q_{ij} are the real and reactive power flow from Bus i to Bus j. r_{ij} and x_{ij} are the series resistance and reactance of the line between Buses i and j. Superscript L notates load and superscript g notates distributed generation. Superscript c notates capacitors. Note that v_i and ℓ_{ij} are the surrogate variables of V_i^2 and I_{ij}^2, whereas the nonequality constraint in (1d) can be relaxed using the second-order cone programming (SOCP) relaxation. The constraint is

$$\ell_{ij} \geq (P_{ij}^2 + Q_{ij}^2)/v_i \tag{2a}$$

$$\left\| \begin{bmatrix} 2P_{ij} & 2Q_{ij} & \ell_{ij} - v_i \end{bmatrix}^T \right\|_2 \leq \ell_{ij} + v_i \tag{2b}$$

For the problem to be implementable, constraint needs to satisfy an equality in order to comply with the physical interpretation. The accuracy of the relaxation is examined in Section III for the problem solution.

2) OLTC Model: An OLTC switches taps in order to adjust the substation voltage. That is, the secondary-side voltage is increased/decreased by changing the turns ratio so as to affect the nodal voltages and power flows of the entire distribution system. Assuming $(i, j) \in \mathcal{E}_{\text{tap}}$ and a set of discrete elements $\mathcal{X} := \{0, 1, \ldots, x_{\max}\}$, the OLTC model is

$$t_{ij} = \left(t^{\min} + \Delta t_{ij} x\right) \tag{3}$$

$$0 \leq x \leq x_{\max} \qquad \Delta t_{ij} = (t_{ij}^{\max} - t_{ij}^{\min})/x_{\max} \tag{4}$$

where t_{ij} is the OLTC ratio, $t_{ij}^{\max}$ and $t_{ij}^{\min}$ are maximum and minimum turns ratios, Δt_{ij} is the change per tap, and $x \in \mathcal{X}$ is the tap position, which takes different discrete values to change the ratio. Since the ratio also takes $|\mathcal{X}|$ of values, the switching process can be exactly represented using binary variables.

$$T_{ij} = \sum_{x=0}^{\mathcal{X}} (t_{ij}^{\min} + \Delta t_{ij} x)^2 u_x \qquad \sum_{x=0}^{\mathcal{X}} u_x = 1 \tag{5}$$

$$v_{ij} = T_{ij} v_i \tag{6}$$

where T_{ij} is composed of squared ratios to be compatible with the voltage variable representation, and binary variables, u_x, whose sum to one forces a selection of one ratio. For example, if the tap position is $x = 5$, then u_5 becomes one to represent the corresponding ratio, while the rest of binary variables are zeros. Heed that (6) is *convex* if the primary-side voltage is known. For OLTCs, the primary side is the substation as in Fig. 2. The tap position can be recovered from the solution as

$$x = (\sqrt{v_{ij}^*/v_i^*} - t_{ij}^{\min})/\Delta t_{ij}$$

3) Switched CB Model: A set of switchable capacitors can be installed at the jth node, where each capacitor is switched on to increase the voltage at the node of installation and adjacent nodes. Assuming $j \in \mathcal{N}_{\text{cap}}$, an integer variable, C_j, is defined to enforce the switching operation.

$$0 \leqslant C_j \leqslant N_c \tag{7}$$

$$q_j^c = Q_c \frac{C_j}{N_c} \tag{8}$$

where q_j^c is the SCBs' variable included in (1b), and Q_c and N_c are the rating and number of the total SCB units; respectively.

4) PV Inverter Model: In order to represent the operating points shown in Fig. 1, the reactive-power constraint is expressed as

$$|q_i^g| \leqslant \sqrt{(s_i^g)^2 - (p_i^g)^2} \tag{9}$$

Overcapacity of the inverter and thus reactive power generation/absorption during peak PV generation are ensured if the nameplate MVA, namely s_i^g, is larger than peak PV active power, p_{max}^g.

5) Voltage Limits: Except for the substation node ($v_0 = V_0^2 = 1$), $\pm 5\%$ of the nominal voltage are enforced as bounds on each node.

$$V_{i\,\min}^2 \leqslant v_i \leqslant V_{i\,\max}^2 \tag{10}$$

6) CVR Limits: The CVR originates from the fact that voltage-dependent loads, i.e. constant impedance or current loads, consume more energy when the voltage is above nominal, increasing annual energy costs. Therefore, CVR practices aim at reducing voltage magnitudes to the lower-half of the allowable limit.

The constraints in (11) are used to keep the voltage of the ith node between minimum and maximum thresholds.

$$z_i \geqslant 0, \quad z_i \geqslant v_i - (V_{i\,\min}^{thr})^2, \quad z_i \geqslant -v_i + (V_{i\,\max}^{thr})^2 \quad (11)$$

This is advantageous as a tighter threshold, i.e. $V_{i\,\max}^{thr} = 1$, can be assigned for nodes at which voltage-dependent loads are installed, $i \in \mathcal{N}_{\text{cvr}}$, and z_i is minimized with large cost coefficients to create a trade-off with the loss-minimization objective. Moreover, this objective can be generalized for all nodes with lower costs and wider limits, say $\pm 3\%$, to flatten the voltage. The desired lower threshold is -3% so as to avoid excessive voltage drop at the point of interconnection and maintain the safety of the equipment behind the meter.

B. Overall VVO Problem

The overall optimization problem over T horizons is formulated as follows.

$$\begin{aligned} \min \quad f = \sum_{t}^{T} \Bigg(& \lambda_{\text{loss}} \sum_{(i,j)\in\mathcal{E}} r_{ij}\ell_{t,ij} + \lambda_{\text{cvr}} \sum_{i\in\mathcal{N}_{\text{cvr}}} z_{t,i} \\ & + \lambda_{\text{flat}} \sum_{i\in\mathcal{N}-\mathcal{N}_{\text{cvr}}} z_{t,i} + \lambda_{\text{cap}} \sum_{i\in\mathcal{N}_{\text{cap}}} |C_{t,i} - C_{t-1,i}| \\ & + \lambda_{\text{tap}} \sum_{(i,j)\in\mathcal{E}_{\text{tap}}} |T_{t,ij} - T_{t-1,ij}| \Bigg) \\ \text{s.t.} \quad & (1), (2), (5) - (11) \end{aligned} \quad (12)$$

III. Case Studies and Numerical Examples

The case studies highlight the following:

1) the impacts of cloudy day and clear day on the frequency of an OLTC's and SCBs' operations.
2) the effectiveness of the centralized VVO to mitigate the equipment operations and adhere to CVR limits by virtue of the inverter's inherent VAR capability.

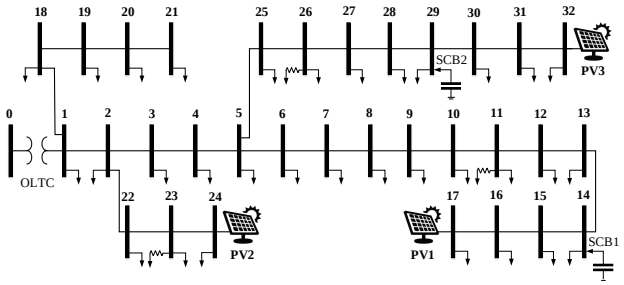

Fig. 3: Modified IEEE 33-node feeder.

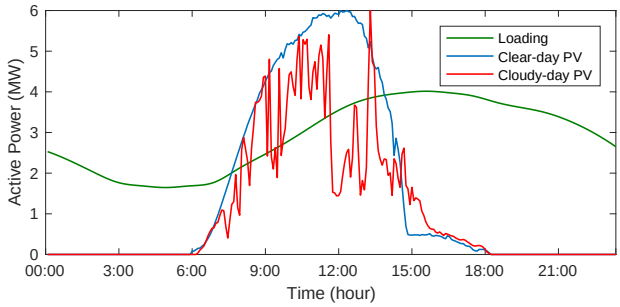

Fig. 4: Loading, clear-day PV and cloudy-day PV profiles.

A. Modified IEEE 33-node feeder

Fig. 3 illustrates the IEEE 33-node feeder, which was modified to include an OLTC, SCBs and voltage-dependent loads. The original peak load is 4.55 MVA with power factor of 0.82. Loads at each node and line parameters are obtained from [14]. Three resistive loads are modeled, each with 100 kW, at nodes 11, 23 and 26. The OLTC is installed on the substation branch, with a turns ratio varying from 0.95 to 1.05. The tap position is constrained by $x_{\max} = 32$, which is a typical limit of a practical tap changer's winding. Also, two SCBs, each with a total of 360 kVAR and three switchable units ($N_c = 3$), are installed at the remote node 14, and the heavy reactive power loaded bus 29, whose adjacent buses (28 and 30) consume 30% of the load.

Fig. 4 shows a loading curve obtained from PJM, and depicted by the total active power load. Also, three 2-MW PV plants are installed at nodes 17, 24 and 32. Each PV inverter has 110% apparent-power capacity of the peak active power. Fig. 4 shows two PV power profiles by the total MW at 5-minute resolution. The profiles mimic a real solar panel's data collected at the University of South Florida on May 15, and August 15 of 2013.

The optimization problem was formulated and solved by the CVX toolbox [15] with MATLAB R2014a, and in conjunction with the GUROBI solver [16].

B. Case Studies and Results

The optimization problem in (12) is solved every 15 minutes, and multiple scenarios are carried out interchangeably. Equipment-operation penalties are fine-tuned starting with small values to achieve the best coordination with PV VARs [2]. For simplicity, loss reduction and CVR objectives are set with unity penalties, while flatness is found to take effect with 0.3.

TABLE I: Cost Coefficients

Objective	Symbol	Range	Cost ($)
Loss Reduction	λ_{loss}	-	1
CVR	λ_{cvr}	0.97-1.00 pu	1
Flat Profile	λ_{falt}	0.97-1.03 pu	0.3
Tap Operations	λ_{tap}	0-32 taps	3
SCB Operations	λ_{cap}	0-3 units each	0.1

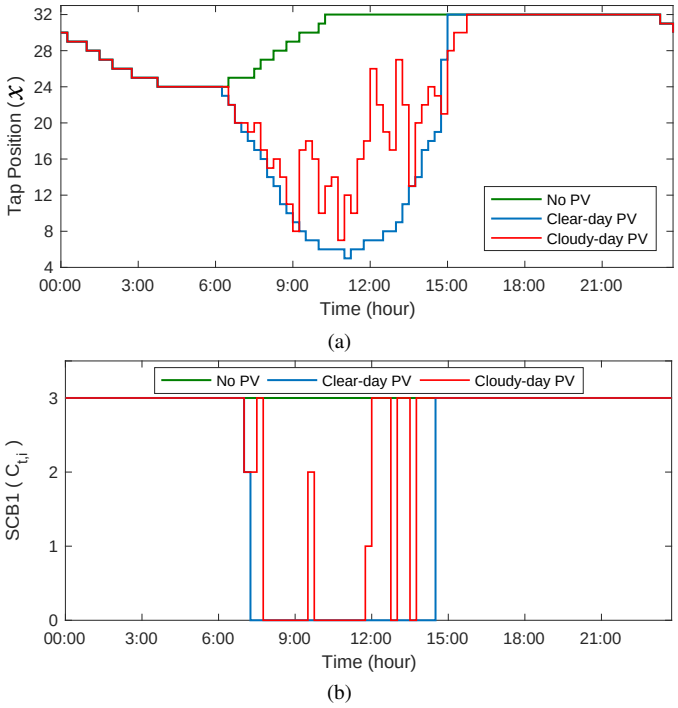

Fig. 5: (a) Tap positions. (b) Number of switched CBs.

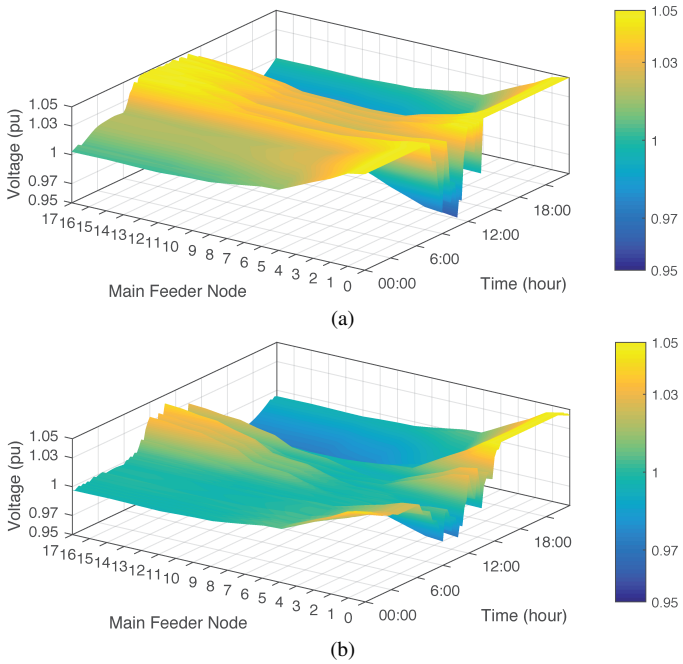

Fig. 6: Main feeder voltages (a) without and (b) with CVR and flat-profile penalties.

TABLE II: Operation Counts at unity PF of PVs

Equipment	No PV	Clear-day PV	Cloud-day PV
Taps	16	36	43
SCB1	-	3	11
SCB2	-	5	8

Case I: At unity power factor of the PV inverters, the three scenarios are compared in terms of equipment operations. Since the inverter's VAR is absent for this case, the tap-cap costs in the VVO are zeroed out ($\lambda_{\text{tap}} = \lambda_{\text{cap}} = 0$) so as to let the OLTC and SCBs satisfy the operation constraints. At no PV, the tap actions are moderate and following the load, while SCBs kept supplying full VARs. However, during both clear-day and cloudy-day PV penetrations, the tap-cap actions dramatically increased in frequency to cope with the dynamic net load. PV power at a cloudy-day in particular results in significant increase of switching actions, and is consequently deemed the worst-case scenario.

Case II: Keeping tap-cap costs zeroed out, the scenario with cloudy-day and unity-PF PVs is solved with and without costs that penalize CVR and flat-profile objectives to explore the capability of traditional equipment to abide by the thresholds of these objectives. The main feeder is selected to examine voltage profiles, which has an OLTC, a resistive load at node 11, switched CBs at node 14, and a PV at node 17. Fig. 6a shows that without the penalties, the loss-reduction objective operates taps and SCB mostly at their maximum bound, thus increasing voltage variations at the downstream nodes and violating CVR. The taps and SCB1 are suddenly reduced when the voltage at node 17 tends to exceed 1.05 pu. On the other hand, with the penalties, Fig. 6b shows that voltages are regulated closely within the desired limits specified in Table I, and with tap-cap actions shown in Table II During evening hours 16:00-21:00, the flatness penalty, λ_{flat}, takes less effect on the OLTC secondary voltage as more taps are switched to counteract the heavy loading. It can be concluded that traditional equipment can effectively regulate voltages within the specified thresholds. This however comes at the cost of increased equipment operations.

Case III: With off-unity power factor PV inverters, the possibility of coordination between traditional equipment and inverters towards reducing tap-cap operations and improving voltage profiles is explored utilizing the multi-objective function in (12) and considering all costs in Table I.

Being the worst-case scenario in terms of equipment operation and voltage variation, the VVO is solved for the cloudy-day PV. The results in Fig. 7 focuses on the period when PV power is most variable.

Fig. 7 shows that when the VVO is solved without the switching penalties, the inverters are not urged to generate/absorb enough VARs so as to reduce the tap-cap actions, since voltages are within the limits as in Fig. 7d. As a result, the switching not only maintains a similar behavior, but also increased for the OLTC and SCB1 as in Table III. Exceptionally, SCB2 remains unswitched without the switching penalty. In contrast, with the switching penalties in Table I, the PV VARs coordinates well with the OLTC taps, while keeping SCB1 unswitched as in the baseline case. The coordination can be observed at instances when PV VARs approach zero, OLTC taps switch with smaller steps than those

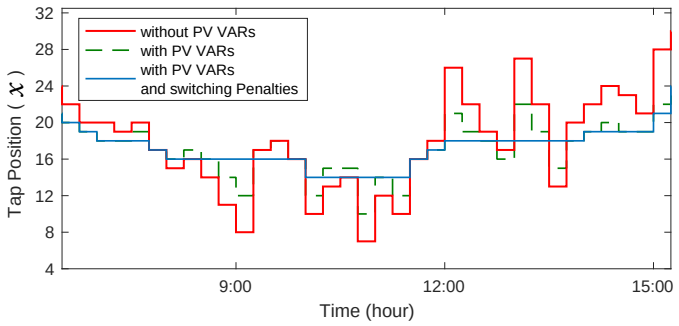

(a)

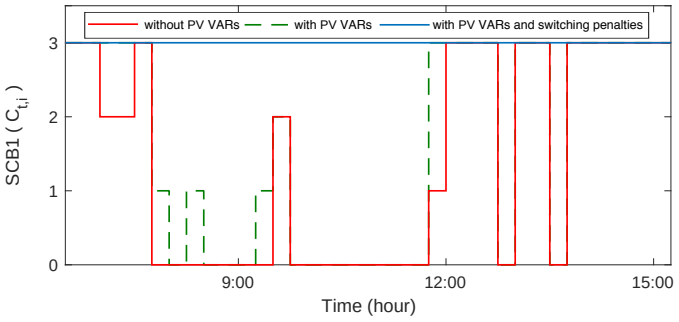

(b)

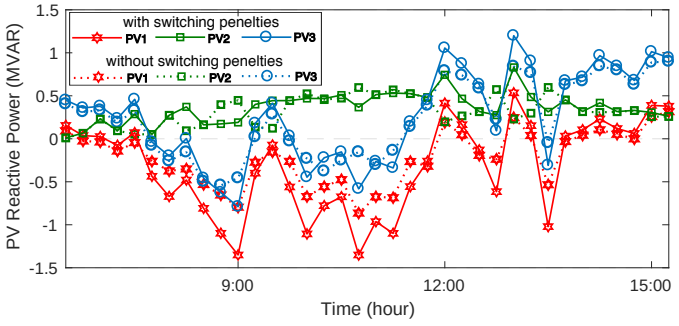

(c)

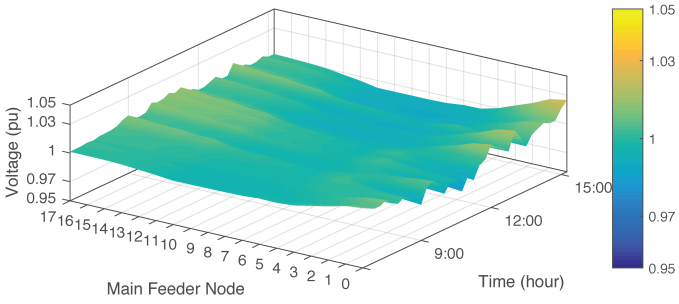

(d)

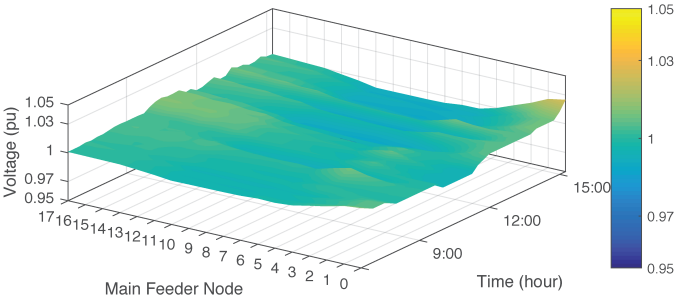

(e)

Fig. 7: (a) Tap positions. (b) Number of switched CBs. (c) VARs from each inverter with and without switching penalties. (d) VAR-compensated main feeder voltages without switching penalties, and (e) with switching penalties.

TABLE III: Cloudy-day Operations at off-unity PF of PVs

Equipment	With PV VARs	With PV VARs & switching penalties
Taps	47	20
SCB1	12	-
SCB2	-	-

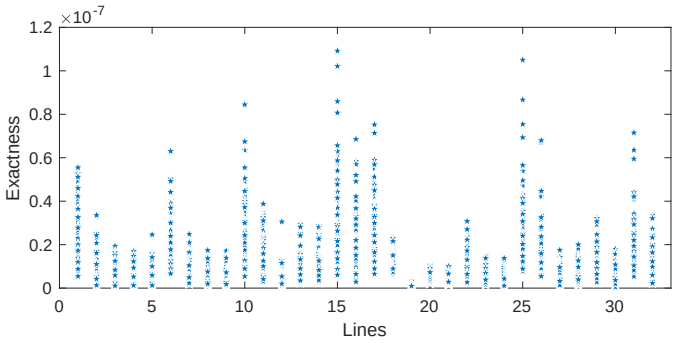

Fig. 8: Exactness of the centralized VVO solution.

simulated without switching penalties and/or VARs.. Also, the reactive/capacitive PV VARs boost to counteract the peaks and valleys of PV active power. The resulting voltage profiles are further improved as in Fig. 7e. Table III lists the switching counts for each device.

C. Exactness of SOCP

The implementability of the presented centralized VVO is verified via examining the exactness of the SOCP relaxation. The SOCP relaxation is said to be exact if the solution admits the power flow characteristics. That is, the inequality constraint of the squared current in (2) satisfies a sufficiently small error. Therefore, the exactness for the solution of all currents and over all time horizons is examined by computing the error in (13). The results are shown in Fig. 8.

$$\text{Exactness} = \sum_{t\in T}\sum_{(i,j)\in\mathcal{E}} |\ell_{t,ij} - (P_{t,ij}^2 + Q_{t,ij}^2)/v_{t,i}| \quad (13)$$

Since the overall errors are in the order of 1×10^{-7}, the solution is exact and the presented VVO is implementable.

IV. Conclusion

This paper formulates a centralized VVO that aims at reducing equipment operations and keeping overall voltage profiles within the satisfactory limit at high penetration of PV. CVR practices are also taken into account. Case studies of three scenarios were conducted to demonstrate the effectiveness of the VVO. At unity power factor of the PV inverters , the results have shown that the traditional equipment approximately fulfilled the specified limits for voltage. This was at the expense of increased and repetitive operations of taps and switched capacitors. By minimizing the switching cost of OLTC taps and switched capacitors, off-unity inverters operate as the fundamental voltage regulators mainly

via boosting reactive-power supply/absorption throughout the variable PV penetration. Therefore, coordination between the traditional equipment and PV inverters can effectively reduce equipment operations, make optimal utilization of DGs, and flatten voltage profiles even at mid-way nodes.

REFERENCES

[1] F. Katiraei and J. R. Aguero, "Solar pv integration challenges," *IEEE Power and Energy Magazine*, vol. 9, no. 3, pp. 62–71, 2011.

[2] Y. P. Agalgaonkar, B. C. Pal, and R. A. Jabr, "Distribution voltage control considering the impact of pv generation on tap changers and autonomous regulators," *IEEE Transactions on Power Systems*, vol. 29, no. 1, pp. 182–192, 2014.

[3] H. Farhangi, "The path of the smart grid," *IEEE power and energy magazine*, vol. 8, no. 1, 2010.

[4] M. Farivar, C. R. Clarke, S. H. Low, and K. M. Chandy, "Inverter var control for distribution systems with renewables," in *Smart Grid Communications (SmartGridComm), 2011 IEEE International Conference on*. IEEE, 2011, pp. 457–462.

[5] M. Nick, R. Cherkaoui, and M. Paolone, "Optimal allocation of dispersed energy storage systems in active distribution networks for energy balance and grid support," *IEEE Transactions on Power Systems*, vol. 29, no. 5, pp. 2300–2310, 2014.

[6] J. Smith, W. Sunderman, R. Dugan, and B. Seal, "Smart inverter volt/var control functions for high penetration of pv on distribution systems," in *Power Systems Conference and Exposition (PSCE), 2011 IEEE/PES*. IEEE, 2011, pp. 1–6.

[7] H. Zhu and H. J. Liu, "Fast local voltage control under limited reactive power: Optimality and stability analysis," *IEEE Transactions on Power Systems*, vol. 31, no. 5, pp. 3794–3803, 2016.

[8] R. Pedersen, C. Sloth, and R. Wisniewski, "Coordination of electrical distribution grid voltage control-a fairness approach," in *Control Applications (CCA), 2016 IEEE Conference on*. IEEE, 2016, pp. 291–296.

[9] M. Farivar and S. H. Low, "Branch flow model: Relaxations and convexification?part i," *IEEE Transactions on Power Systems*, vol. 28, no. 3, pp. 2554–2564, 2013.

[10] M. Baran and F. F. Wu, "Optimal sizing of capacitors placed on a radial distribution system," *IEEE Transactions on power Delivery*, vol. 4, no. 1, pp. 735–743, 1989.

[11] L. Bai, J. Wang, C. Wang, C. Chen, and F. F. Li, "Distribution locational marginal pricing (dlmp) for congestion management and voltage support," *IEEE Transactions on Power Systems*, 2017.

[12] W. Wu, Z. Tian, and B. Zhang, "An exact linearization method for oltc of transformer in branch flow model," *IEEE Transactions on Power Systems*, vol. 32, no. 3, pp. 2475–2476, 2017.

[13] L. H. Macedo, J. F. Franco, M. J. Rider, and R. Romero, "Optimal operation of distribution networks considering energy storage devices," *IEEE Transactions on Smart Grid*, vol. 6, no. 6, pp. 2825–2836, 2015.

[14] M. E. Baran and F. F. Wu, "Network reconfiguration in distribution systems for loss reduction and load balancing," *IEEE Transactions on Power delivery*, vol. 4, no. 2, pp. 1401–1407, 1989.

[15] M. Grant, S. Boyd, and Y. Ye, "Cvx: Matlab software for disciplined convex programming," 2008.

[16] I. Gurobi Optimization, "Gurobi optimizer reference manual; 2015," *URL http://www. gurobi. com*, 2016.